Parameterization, Analysis & Simulation of a Heat Gun

Submitted by

Thomas A. Bowers

December 10, 2002

2.141: Modeling and Simulation of Dynamic Systems
Fall 2002
Massachusetts Institute of Technology

1 Introduction

This paper discusses the dynamic analysis and simulation of a heat gun. The system consists of an electric heating coil and a universal AC electric motor that drives a centrifugal fan in order to produce airflow. A diagram of the system is shown in Figure 1. Although the system looks relatively simple there are complex interactions between electrical, mechanical, thermal, and fluid domains.

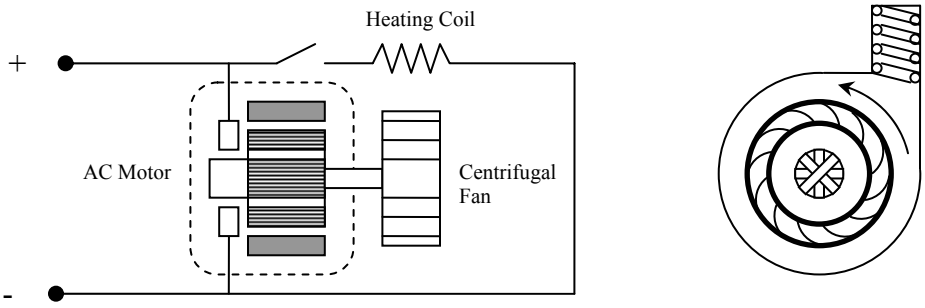

Figure 1: Schematic of Heat Gun

2 System Model

Because the system operates in four domains there are several couplers required to convert energy from one domain into energy in another domain.

2.1 Electro-mechanical Coupling

The coupling between electrical and mechanical domains is the universal AC motor. A diagram of the universal motor is shown in Figure 2. Because the windings on the rotor are connected in series with windings on the two poles of the stator, this motor is able to

Schematic and graph removed due to copyright considerations.
See reference [1].

Figure 2: Universal Motor Wiring Diagram and τ-N Curve

operate with an AC or DC power supply [1]. This allows the motor to be treated similarly to a simple DC motor, which is modeled as a linear gyrator. The motor constant, K_m, can be determined experimentally by measuring the input voltage and current when driving the motor at a known speed. It is evident from part b of Figure 2 that AC operation is

even more linear than DC operation for this type of motor adding validity to the use of a linear gyrator.

2.2 Electro-thermal Coupling

The interaction between the electrical domain and the fluid domain is a thermal coupling. To transfer energy to the fluid, the material of the electrical resistor must first heat up. The coupling is modeled as a non-conservative two-port resistor. This is due to the fact that electrical energy is converted to thermal energy, but thermal energy does not create electrical energy. The power dissipated in the resistor is equal to e^2/R. This power is converted to thermal energy through the generation of entropy. Thermal energy is stored in the resistor, which acts as a thermal capacitor, and transferred to the air by convection.

2.3 Thermo-Fluid Coupling

The thermal energy that is transferred through convection can be modeled using the *HRS* macro element that is presented in Brown [2]. This bond is used to model heat exchangers and allows the heater temperature to be much larger than the temperature of the fluid at the inlet or outlet port.

2.4 Mechanical-Fluid Coupling

The centrifugal fan provides the coupling between mechanical and fluid domains. The geometry of the fan used in this heat gun is a forward-curved blade centrifugal blower, which is also known as a sirocco fan. As with the coupling between electrical and fluid domains, the mechanical to fluid transmission requires a non-conservative coupler modeled as a two-port resistor. Losses in the fan are due to vorticity, friction, and turbulence. An efficiency coefficient, η, can be used to account for these losses in the fan.

2.5 System Bond Graph

After determining the necessary transmission elements of the system, it is possible to create the bond graph of the system, which is shown below in Figure 3.

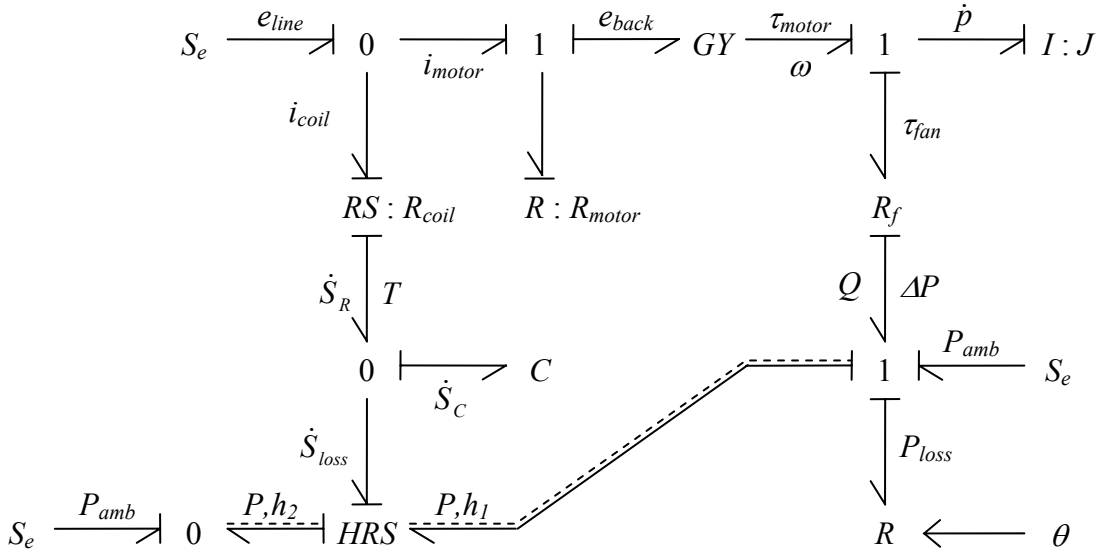

Figure 3: Bond Graph Representation of Heat Gun

2.6 System Equations

Because the heat gun has a parallel circuit, it is possible to analyze much of the system as two separate networks. The output of the motor-fan system, which is the airflow through the heat gun, can be determined independent of the thermal characteristics of the system. The thermal response of the system is dependent on the transient in the flow rate; however, the flow rate transient is much faster than the heat coil transient.

The equations for the fan are the most difficult to derive, but they can be determined based on conservation of momentum [3]. The rate of change of fluid angular momentum is equal to the torque applied on it:

$$\tau_{fan} = \frac{dH_0}{dt} = \frac{d}{dt}\int (V \times r)dm = \dot{m}(V_{\theta 2} r_2 - V_{\theta 1} r_1)$$

For the system blade geometry the velocity diagrams shown in Figure 4 are used to determine $V_{\theta 2}$ and $V_{\theta 1}$.

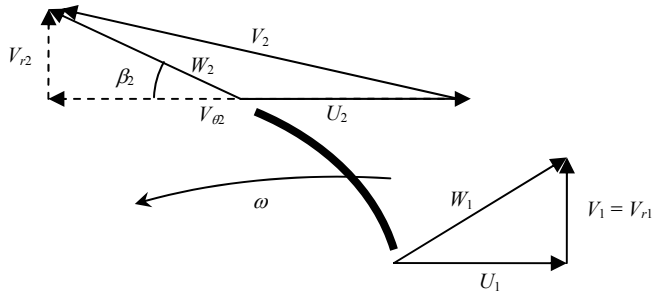

Figure 4: Velocity Diagrams for Inlet and Outlet Flow of Centrifugal Fan

From Figure 4 it is evident that the $V_{\theta 2}$ is equal to:

$$V_{\theta 2} = U_2 + V_{r2}\cot\beta_2 = r_2\omega + \frac{Q\cot\beta_2}{2\pi r_2 b_2}$$

where $2\pi r_2 b_2$ is the area of the fan outlet and Q is the volumetric flowrate.

The flow into the fan is assumed to be purely radial, which gives $V_{\theta 1} = 0$. Substituting these velocities back into the torque equation results in the following expression:

$$\tau_{fan} = \dot{m} r_2 \left(r_2\omega + \frac{Q\cot\beta_2}{2\pi r_2 b_2} \right) = \rho Q r_2 \left(r_2\omega + \frac{Q\cot\beta_2}{2\pi r_2 b_2} \right)$$

From this is clear that the fan torque is dependent both on volumetric flowrate and angular velocity. This is consistent with non-conservative two-port resistors, which supports the use of this type of coupling in the system bond graph. However, the torque equation does not account for losses in the fan. The forward-curved blade geometry is not

as efficient as a backward-curved blade or an airfoil [4]. Therefore, the fan torque needs to be divided by the fan efficiency in order to model its non-conservative nature.

$$\tau_{fan} = \frac{\rho Q r_2}{\eta}\left(r_2\omega + \frac{Q\cot\beta_2}{2\pi r_2 b_2}\right)$$

The pressure rise in the fan is determined from the conservation of energy (with the efficiency loss taken into account).

$$\tau_{fan}\omega = \Delta P Q \Rightarrow \Delta P = \frac{\rho\omega r_2}{\eta}\left(r_2\omega + \frac{Q\cot\beta_2}{2\pi r_2 b_2}\right)$$

The pressure rise in the fan is equal to the pressure lost as the air travels through the heat gun. An adjustable orifice varies the inlet area allowing for control of the flowrate. Additional restrictions in the flow path include the heating coil and wall friction along the length of the flow path [5].

$$\Delta P = \rho\frac{V_2^2 - V_1^2}{2} + h_l = \frac{\rho}{2}\left(\left(\frac{Q}{A_2}\right)^2 - \left(\frac{Q}{A_1(\theta)}\right)^2\right) + \sum_{i=2}^{n} f_i \frac{\rho}{2}\frac{L_i}{D_i}\left(\frac{Q}{A_i(\theta)}\right)^2$$

$$\Delta P = \frac{\rho}{2}Q^2\left(\frac{A_2^2 - A_1^2}{A_2^2 A_1^2} + \sum_{i=2}^{n} f_i \frac{L_i}{D_i}\frac{1}{A_i^2}\right) = \frac{\rho}{2}\frac{Q^2}{A_e{}^2}$$

where, f_i, L_i, and D_i are the friction factor, length, and diameter of the i^{th} restriction section, respectively, and A_e is the effective area of the entire system.
The ratio L/D, also known as the effective length, is provided for various pipe geometries, valves, and other types of restrictions.

The preceding expression for ΔP is in terms of Q only; however, ΔP found from the energy balance equation also included the angular velocity of the fan, ω. Therefore, Q can be solved in terms of the angular velocity, ω:

$$\frac{\rho\omega r_2}{\eta}\left(r_2\omega + \frac{Q\cot\beta_2}{2\pi r_2 b_2}\right) = \frac{\rho}{2}\frac{Q^2}{A_e{}^2} \Rightarrow \left(\frac{\eta}{2\omega r_2 A_e^2}\right)Q^2 - \frac{\cot\beta_2}{2\pi r_2 b_2}Q - \omega r_2 = 0$$

$$Q = \frac{\dfrac{\cot\beta_2}{2\pi r_2 b_2} + \sqrt{\left(\dfrac{\cot\beta_2}{2\pi r_2 b_2}\right)^2 + \dfrac{2\eta}{A_e^2}}}{\dfrac{\eta}{\omega r_2 A_e^2}}$$

The angular velocity is related to the state variable, p, by the following equation:

$$\omega = \frac{p}{J}$$

The remaining equations needed to solve for the system dynamics are provided by the motor equations and the state equation for angular momentum, *p*:

$$e_{back} = K_m \omega$$
$$i_{motor} = \frac{e_{line} - e_{back}}{R_{motor}}$$
$$\tau_{motor} = K_m i_{motor}$$

$$\dot{p} = \tau_{motor} - \tau_{fan}$$

The thermal component of the heat gun behavior is determined from the equations for the *HRS* macro element and the conversion of electrical energy into thermal energy. The thermal equations are as follows:

$$T_{coil} = T_0 e^{\frac{S_C - S_0}{mc}}$$
$$\mathcal{P} = \frac{e_{line}^2}{R_{coil}} = T_{coil}\dot{S}_R \Rightarrow \dot{S}_R = \frac{e_{line}^2}{T_{coil}R_{coil}}$$
$$\dot{S}_{loss} = \frac{1 - T_{amb}/T_{coil}}{1/H + 1/c_p\dot{m}} = \frac{1 - T_{amb}/T_{coil}}{1/H + 1/c_p\rho Q}$$
$$\dot{S}_C = \dot{S}_R - \dot{S}_{loss}$$

3 System Parameterization

In order to simulate the heat gun, the system parameters were determined through measurement and experimentation. The following subsections discuss the methods used to determine the system parameters.

3.1 Fan Parameters

Most of the parameters associated with the fan involved its geometry, as indicated by the velocity diagrams in Figure 4. The dimensions of the fan and its blades were measured, and the blade angle at the outlet estimated by assuming that the blade formed the arc of a circle. According to Logan [6], the maximum efficiency of centrifugal fans varies from 70 to 90 percent. Logan also provides a table relating centrifugal fan efficiency to volumetric flow rate. The logarithmic regression from his table provides the following relationship between flow rate and efficiency:

$$\eta = 0.0722 \ln(Q) + 0.5638$$

For this application the flow rate is probably on the order of 0.5 L/s, which leads to an efficiency of about 50%. Therefore, the fan parameters are as follows:

```
%Fan Parameters
r1=.03066;                  %Inlet Blade Raidus, m
B1=59.27*pi/180;            %Inlet Blade Angle, rad
b1=.01;                     %Inlet Height, m
r2=.0375;                   %Outlet Blade Radius, m
B2=10*pi/180;               %Outlet Blade Angle, rad
b2=.01;                     %Outlet Height, m
eta=.50;                    %Fan Efficiency
```

3.2 Flow Parameters

The flow parameters were the most difficult to determine by measurement. While the geometries of the inlet and exit were easy to measure, the internal restrictions in the heat gun posed a problem. The inlet and outlet were treated as lossless elements in the flow path, only contributing to the calculation of velocity into and out of the system for Bernoulli's equation. To determine the pressure losses due to the flow within the heat gun, two major sources of loss were considered. The first was the loss associated with the flow directional change due to the fan volute. Fox and McDonald [5] provide a graphical estimation for losses associated with 90º pipe bends that is based on the ratio of the radius of curvature to the diameter of the pipe, r/D. For this system the ratio is ~3, which results in an effective length, L_e/D, of about 13. This value is multiplied by 3 to account for 270º of volute bend. The volute pressure loss is also proportional to the loss coefficient, which is determined by the Reynolds number and the Blasius correlation for turbulent flow in smooth pipes:

$$f = \frac{0.316}{Re^{0.25}}$$

The second, and more significant loss of pressure within the heat gun, is the restriction due to the heating coil. The coil significantly reduces the diameter of the pipe for a length of 10cm just before the outlet. In addition to this significant reduction in diameter, the coil also creates fully turbulent flow in this section of the heat gun. Both of these effects result in huge losses, which are difficult to determine analytically. Therefore, this parameter, which was identified as the effective length of the coil, was left as a variable to be optimized in the simulation. This parameter also accounts for other losses in the fan including the losses at the inlet and outlet that were neglected. The complete set of flow parameters used in the simulation are as follows:

```
%Flow Parameters
Douter=.0670;               %Intake Outer Diameter, m
Dinner=.0320;               %Intake Inner Diameter, m
Ain=pi*(Douter^2-Dinner^2)/4%Maximum Intake Area, m^2
A1=cos(6*theta)*Ain/2;      %Restricted Intake Area, m^2
D2=.029;                    %Outlet Diameter, m
A2=pi*D2^2/4;               %Outlet Area, m^2
rho=1.19;                   %Assume Constant Density, kg/m^3
mu=2e-5;                    %Dynamic Viscosity of Air, Ns/m^2
Dduct=.0145;                %Volute Diameter, m
Aduct=pi*Dduct^2/4;         %Duct Area, m^2
Re=rho*.01/Aduct*Dduct/mu;  %Reynolds Number in Duct (Assume 1 L/s flow)
```

```
fduct=.316/Re^.25;          %Duct Friction Factor (Blasius)
fcoil=.015;                 %Coil Friction Factor
Lduct=13*3;                 %Effective Length of Duct, L/D
Lcoil=550;                  %Effective Length of Coil, L/D
Acoil=A2/2;                 %Effective Coil Area, m^2
A=(A2^2-A1^2)/(A1^2*A2^2)+fduct*Lduct/Aduct^2+fcoil*Lcoil/Acoil^2;
```

3.3 Motor Parameters

The motor parameters were fairly easy to determine, though measurements were made under several different operating conditions to fully characterize the system. The easiest parameter to measure was the resistance of the motor windings, though this varied from 70 to 75 Ω depending on the angle of the motor shaft. Because the system incorporated a universal motor, its parameterization was simplified by utilizing a DC power supply. By applying a known voltage and recording steady-state current draw and shaft speed, it was possible to determine the motor constant, K_m, and therewith the motor torque. The motor speed was measured with a timing gun. K_m is plotted versus applied voltage in Figure 5 below for two operating conditions: no restriction (cover removed), and minimum restriction (A_1=A_{in}).

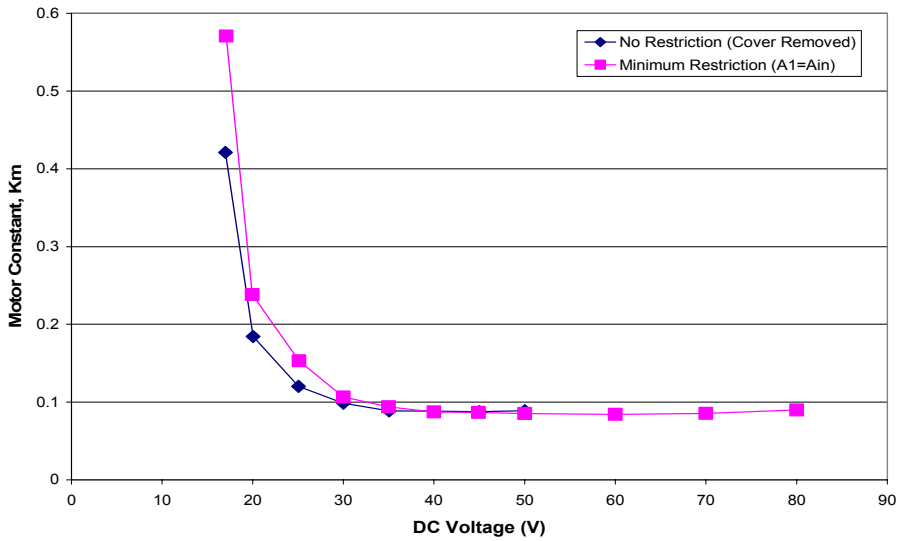

Figure 5: Motor Constant, K_m, versus DC Voltage

For increasing voltage the value of K_m decays to about 0.9 Nm/A. However, it was shown in Figure 2b that AC operation yields slightly different values for K_m. Therefore, the steady-state current and speed were also measured for 120VAC. This resulted in K_m equal to 0.114 Nm/A, which is about 25% larger than the motor constant corresponding to DC operation.

In reality there is a thermal transient in the motor as the rotor and stator heat up due to electrical losses. This results in a slight decay in the current draw that was observed to stabilize completely after about a minute. The decrease in current during this transient was not included in the simulation because it was very small (~10mA). Additionally, the

motor resistance was measured immediately after running in order to capture the true steady-state characteristics of the system.

The DC measurements were also used in characterizing the low-speed characteristics of the motor. The steady-state operating torque was found for each of the points on Figure 5 and plotted versus the motor speed. This resulted in the torque-speed curve of the load, which is shown below in Figure 6.

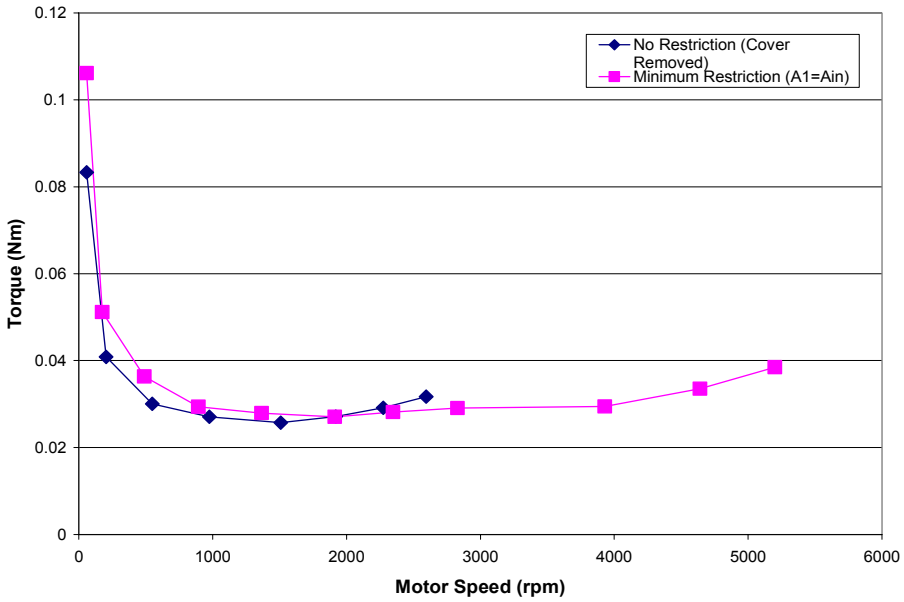

Figure 6: Load Torque versus Motor Speed

This figure is very informative because of the information it contains about motor friction. At low speed operation, one would expect the contribution of torque due to flow rate to be negligible. Therefore, at low speeds the load torque is dominated by motor friction. Judging from the figure, the load torque at 500 to 1500 rpm is entirely due to kinetic friction; beyond this range, the air flow begins to add to the motor load at a quadratic rate. This provides the parameter for motor friction, which is assumed to provide a constant resistive torque (independent of motor speed). This value is not shown on the bond graph, but it would be represented by a constant effort source applied at the ω 1-junction for $\tau_{motor} > \tau_{friction}$. The motor parameters are as follows:

```
%Motor Parameters
eline=120;                  %Line Voltage, Vrms
Rmotor=72.5;                %Motor Coil Resistance, Ohms
Km=.114;                    %Motor Constant, Nm/Amp
J=.0001;                    %Rotatioinal Inertia, kg/m^2
tau0=.03;                   %Motor Friction, Nm
```

3.4 Heat Coil Parameters

The heat coil parameters were very easy to measure. An ohmmeter was used to find the resistance of the coil, which was then weighed to determine its mass. The coil was assumed to be Nichrome (80%-Ni, 20%-Cr) and the specific heat was found in Incropera

and DeWitt [7]. The value for the initial entropy of the coil does not affect the result. The only value dependent on the coil entropy is the coil temperature, and since temperature is dependent on the difference between the instantaneous entropy and the initial entropy the initial value is arbitrary.

```
%Heat Coil Parameters
Rcoil=6;                    %Heat Coil Resistance, Ohms
m=.05;                      %Heat Coil Mass, kg
c=385;                      %NiChrome Specific Heat, J/kg_K
S0=0;                       %Initial Entropy Condition
```

3.5 Fluid Convection Parameters

The inlet air was assumed to be at standard temperature and pressure. Therefore, the only variable that was needed for the simulation was the convection coefficient. In order to determine this constant, the thermal behavior of the heat gun was measured using a thermocouple. The following two plots, Figure 7 and Figure 8, show the temperature of the exhaust air for two operating conditions: maximum inlet area and minimum inlet area.

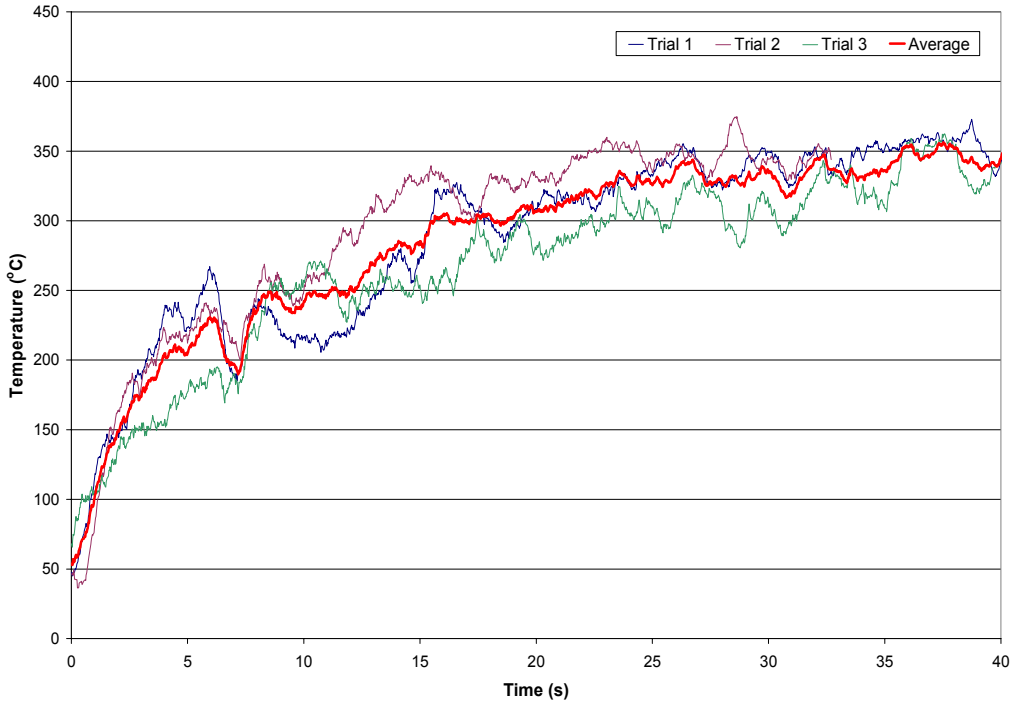

Figure 7: Exhaust Air Temperature with Maximum Inlet Area

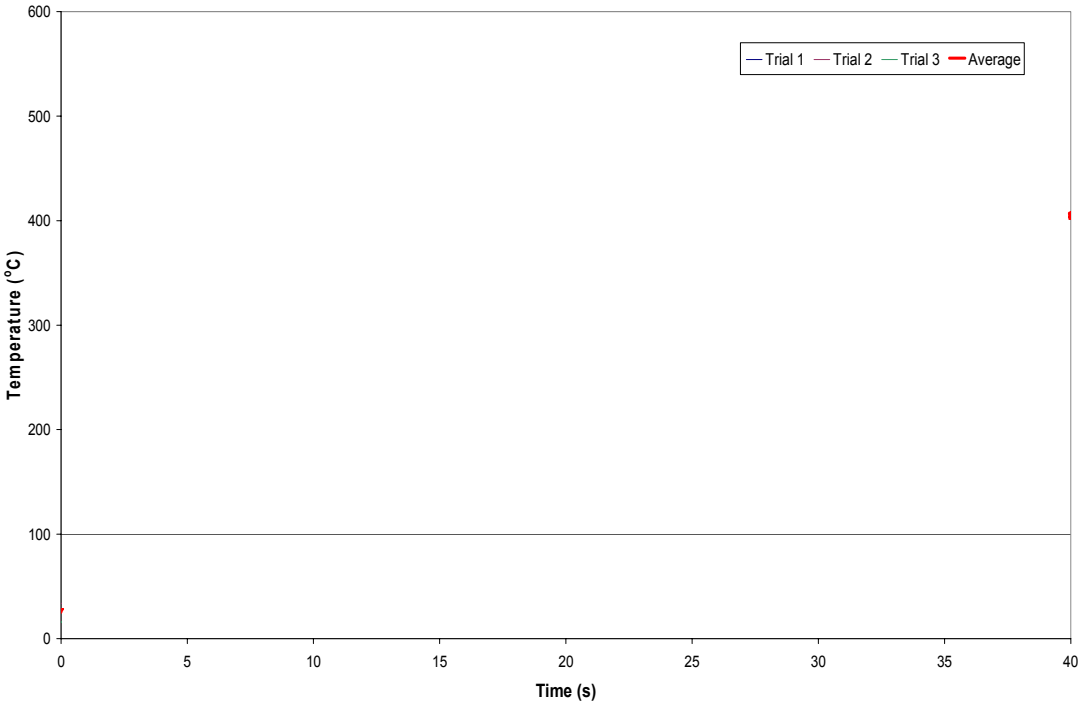

Figure 8: Exhaust Air Temperature with Minimum Inlet Area

From the preceding figures it is clear that reducing the inlet area increases the output temperature. This is due to the fact that convection is dependent on the mass flow of air and the flow rate depends on the inlet area. These two figures can be used to adjust the value of *H* in the simulation.

```
%Fluid Convection Parameters
Tamb=297;                   %Ambient Temperature, K
Pamb=101325;                %Ambient Pressure, Pa
cp=1004;                    %Air Specific Heat @ Constant Pressure, J/kg_K
H=4.5;                      %Bulk Convection Constant, J/K
```

4 System Simulation

Using the parameters defined in Section 3 and the constitutive equations from Section 2.6, the following MATLAB input was used to simulate the dynamic behavior of the heat gun:

```
%2.141 Term Project
%Simualtion of a Heat Gun

clear all
global r2 eline Rmotor Rcoil Km Tamb S0 m c H cp rho J Vt2 eta A omegaout tauout tau0

%j=1;
for j=1:2
    theta=14*(j-1)*pi/180;
%theta=input('What is the Restriction Plate Angle (0-14)?')*pi/180;

Q1(j)=fzero(@solveQ,[1e-20 .02]);
```

```
omega1(j)=omegaout;
tau1(j)=tauout;

tau=[Km*eline/Rmotor 0];
omega=[0 eline/Km*30/pi];

%ODE Solver
t=0:.1:40;
[T,X]=ode45('heatgun_dot',t,[1e-10 S0]);

%Shaft Angular Speed
Omega(:,j)=X(:,1)/J;

for i=1:length(X)

    %Volumetric Flow Rate
    Q(j,i)=(r2*Vt2+sqrt((r2*Vt2)^2+2*eta*A*r2^2))/(eta*A*J/X(i,1));

    %Fan Load
    tau_fan(j,i)=rho*Q(j,i)*(r2*(r2*Omega(i,j)+Q(j,i)*Vt2))/eta;

    %Exhaust Air Temperature
    Tcoil(j,i)=Tamb*exp((X(i,2)-S0)/(m*c));
    Sloss_dot(i)=(1-Tamb/Tcoil(j,i))/(1/H+1/(cp*rho*Q(j,i)));
    Qdot(i)=Tcoil(j,i)*Sloss_dot(i);
    Tair2(j,i)=Tamb+Qdot(i)/(cp*rho*Q(j,i))-273.15;

    %Motor Current
    eback(i)=Km*Omega(i,j);
    imotor(j,i)=(eline-eback(i))/Rmotor;

end

close all
if j==2
    figure
    plot(omega1(1)*30/pi,tau1(1),'bo',omega1(2)*30/pi,tau1(2),'ro')
    hold on

    plot(omega,tau,'k--')
    xlabel('Shaft Speed, (rpm)')
    ylabel('Torque, (Nm)')
    title('Torque-Speed Curve for Motor Indicating Steady-State Operation Points')
    legend('\theta = 0 deg (max area)','\theta = 14 deg (min area)')

    figure
    plot(Omega(:,1)*30/pi,tau_fan(1,:),'b',Omega(:,2)*30/pi,tau_fan(2,:),'r',omega,tau-
    tau0,'k--')
    xlabel('Fan Speed, (rpm)')
    ylabel('Load Torque, Nm')
    title('Load Torque versus Speed for Minimum and Maximum Inlet Area')
    legend('\theta = 0 deg (max area)','\theta = 14 deg (min area)')

    figure
    plot(T,Omega(:,1)*30/pi,'b',T,Omega(:,2)*30/pi,'r')
    xlabel('Time, (s)')
    ylabel('Shaft Speed, (rpm)')
    title('Motor Speed versus Time')
    legend('\theta = 0 deg (max area)','\theta = 14 deg (min area)')

    figure
    plot(T,Q(1,:)*100,'b',T,Q(2,:)*100,'r')
    xlabel('Time, (s)')
    ylabel('Volumetric Flowrate, (L/s)')
    title('Volumetric Flowrate, Q, versus Time')
    legend('\theta = 0 deg (max area)','\theta = 14 deg (min area)')

    figure
    plot(T,Tcoil(1,:)-273.15,'b',T,Tcoil(2,:)-273.15,'r')
    xlabel('Time, (s)')
    ylabel('Heat Coil Temperature, (decC)')
```

```
    title('Heat Coil Temperature for Minimum and Maximum Inlet Area')
    legend('\theta = 0 deg (max area)','\theta = 14 deg (min area)')

    figure
    plot(T,Tair2(1,:),'b',T,Tair2(2,:),'r')
    xlabel('Time, (s)')
    ylabel('Exhaust Air Temperature, (degC)')
    title('Exhaust Air Temperature for Minimum and Maximum Inlet Area')
    legend('\theta = 0 deg (max area)','\theta = 14 deg (min area)')

    figure
    plot(T,imotor(1,:),'b',T,imotor(2,:),'r')
    xlabel('Time, (s)')
    ylabel('Motor Current, (A)')
    title('Motor Current for Minimum and Maximum Inlet Area')
    legend('\theta = 0 deg (max area)','\theta = 14 deg (min area)')

end
end
```

The first function called on by the preceding file was an early solution to the problem that ignored the inertia of the motor and fan. It was, therefore, a zero order system providing the steady-state behavior of the motor and fan. The function 'solveQ' is shown below:

```
function solveQ=f(Q)

global r2 eline Rmotor Km rho Vt2 eta A omegaout tauout tau0

tauout=(r2^2*eline/Km+Q*r2*Vt2)/(eta/(rho*Q)+r2^2*Rmotor/Km^2)+tau0;
omegaout=eline/Km-Rmotor*tauout/Km^2;
P=rho*omegaout*(r2*(r2*omegaout+Q*Vt2))/eta;
solveQ=sqrt((1/A)*2*P/rho)-Q;
```

The second function that is solved by the main function is the set of differential equations for the system:

```
function heatgun_dot=f(t,x)

global r2 eline Rmotor Rcoil Km Tamb S0 m c H cp rho J Vt2 eta A tau0

heatgun_dot=[0 0]';

p=x(1);
Scoil=x(2);

w=p/J;
Q=(r2*Vt2+sqrt((r2*Vt2)^2+2*eta*A*r2^2))/(eta*A/w);
tau_fan=rho*Q*(r2*(r2*w+Q*Vt2))/eta;
tau_motor=Km*(eline-Km*w)/Rmotor;
p_dot=tau_motor-tau_fan-tau0;

mdot=Q*rho;
Tcoil=Tamb*exp((Scoil-S0)/(m*c));
Sloss_dot=(1-Tamb/Tcoil)/(1/H+1/(cp*mdot));
Sr_dot=eline^2/(Rcoil*Tcoil);
Scoil_dot=Sr_dot-Sloss_dot;

heatgun_dot(1)=p_dot;
heatgun_dot(2)=Scoil_dot;
```

4.1 Simulation Results

The simulation was run for θ equal to 0° and 14°, which correspond to the maximum and minimum inlet areas achievable by adjustment of the restriction plate, respectively. The

following results show the outstanding correlation between the mathematical simulation and the recorded data. The first simulation output, Figure 9 below, shows the motor torque versus speed. This line can be drawn without simulation using the parameter K_m, which was found through experimentation.

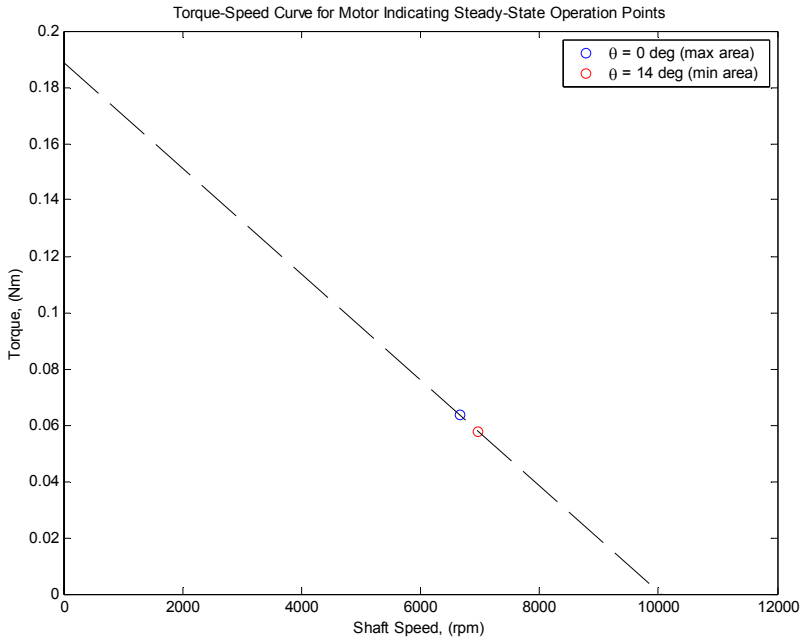

Figure 9: Motor Torque-Speed Curve (Linear K_m) Including Steady-State Speeds for Minimum and Maximum Inlet Area

The blue and red circles on the plot are also determined from the zero dynamics of the system. Because the system is first order, with only a very small inertance due to the motor rotor and fan, the majority of the system operation is at steady-state. The blue circle on the plot, which indicates the steady-state motor speed and torque for the maximum inlet area configuration, is at 6669 rpm. This is less than 0.3% larger than the measured steady-state speed of 6650 rpm. The red circle corresponds to a smaller inlet area and therefore a lower flow rate. Because less momentum is transferred from motor to fluid due to the reduced flow, the resulting torque is lower and the speed is higher. An experimental value of this motor speed could not be measured for this geometry because the restriction plate completely covered the fan preventing the use of the timing gun. However, the current drawn by the motor was measured for both of these conditions (it was used to determine the motor constant for the first configuration) and can be used to calculate the steady-state torque and speed.

For the high speed operation with the restriction fully closed, the current draw was 530mA. This results in 0.06043 Nm of torque at a speed of 6832 rpm. The MATLAB output for this configuration was 6970 rpm, which is only 2% larger than the value calculated by the current measurement.

The following two plots, Figure 10 and Figure 11, show the transients in the motor speed and current. Because of the low motor and fan inertia the system is able to reach steady-state speed in just a few seconds.

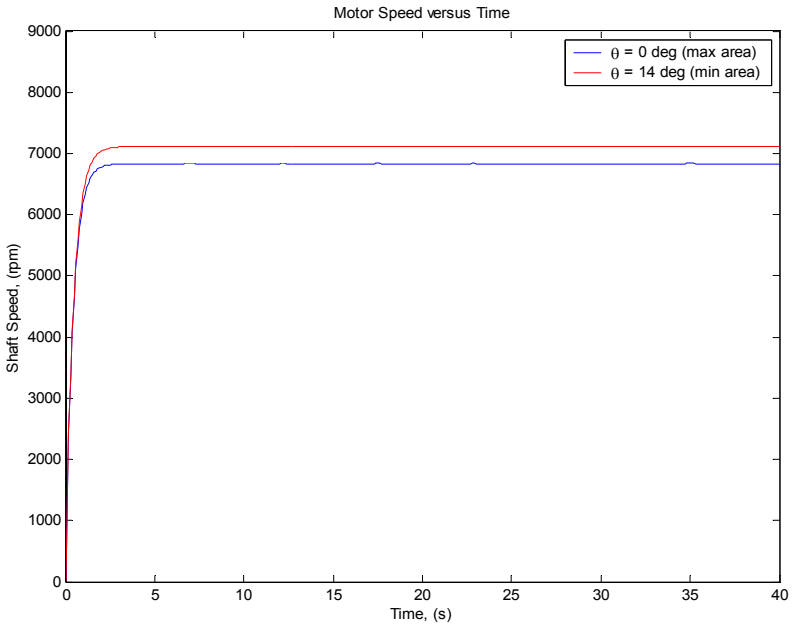

Figure 10: Motor Speed for Dynamic Simulation of Heat Gun

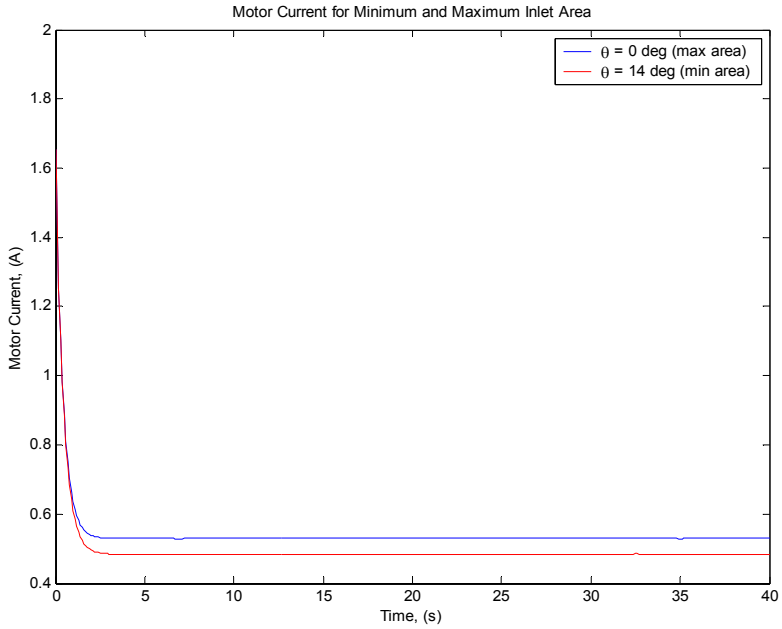

Figure 11: Motor Current for Dynamic Simulation of Heat Gun

Figure 12 shows the volumetric flow rate of the heat gun in Liters per seconds for both operating regimes. Substituting the steady-state flow values back into the equation for

centrifugal fan efficiency from Section 3.1 gives efficiency values of 52% for the fully restricted fan and 53% for the fully opened fan. These values are only a fraction higher than the value of 50%, which was used in the simulation.

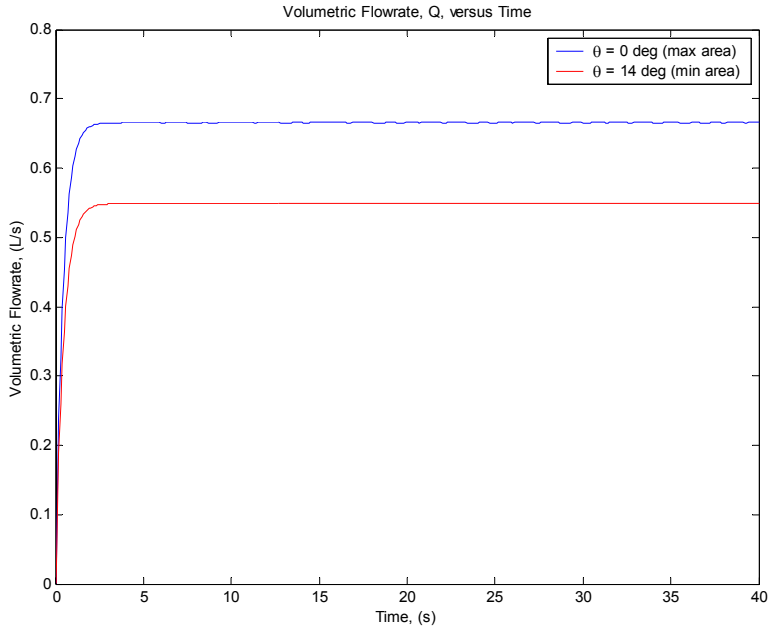

Figure 12: Volumetric Flow Rate for Dynamic Simulation of Heat Gun

While an accurate measurement of flow rate was not made, the experimental load versus speed curve shown previously in Figure 6 illustrated how flow rate contributes quadratically to the load. A similar result is seen in Figure 13, which shows both the shaft load and the motor torque versus speed, which is directly proportional to flow rate.

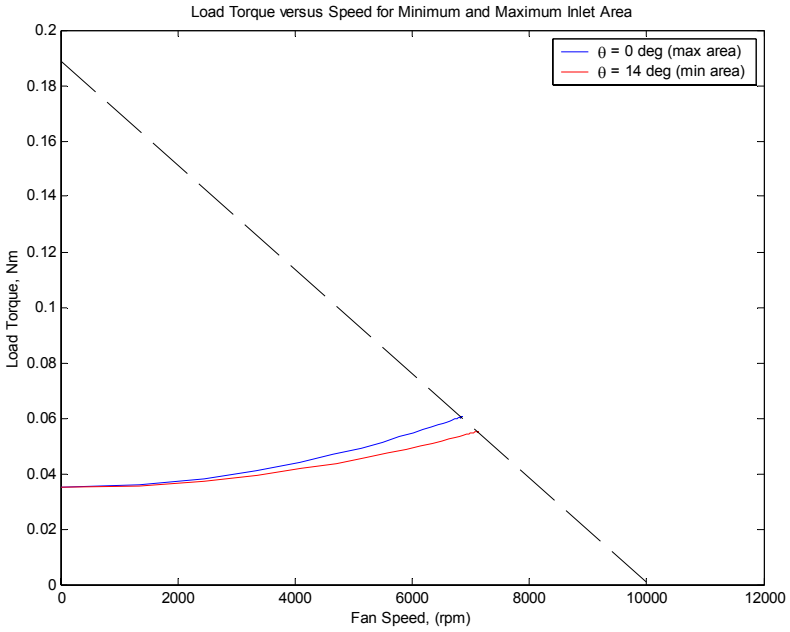

Figure 13: Load Curve and Motor Torque-Speed Curve

Finally, the thermal aspects of the heat gun were addressed. Figure 14 shows the simulated exhaust air temperature for each of the system configurations considered. The time constant of the thermal behavior was modified by adjusting the convection coefficient. The temperature could be scaled by changing the effective length of the flow restrictions in order to decrease volumetric flow rate. Of course this affects the steady-state current and speed, which were known values. The following plot represents the optimized model of the system, which was constrained to meet the known speed and current parameters while also attempting to simulate the thermal data shown in Figure 15.

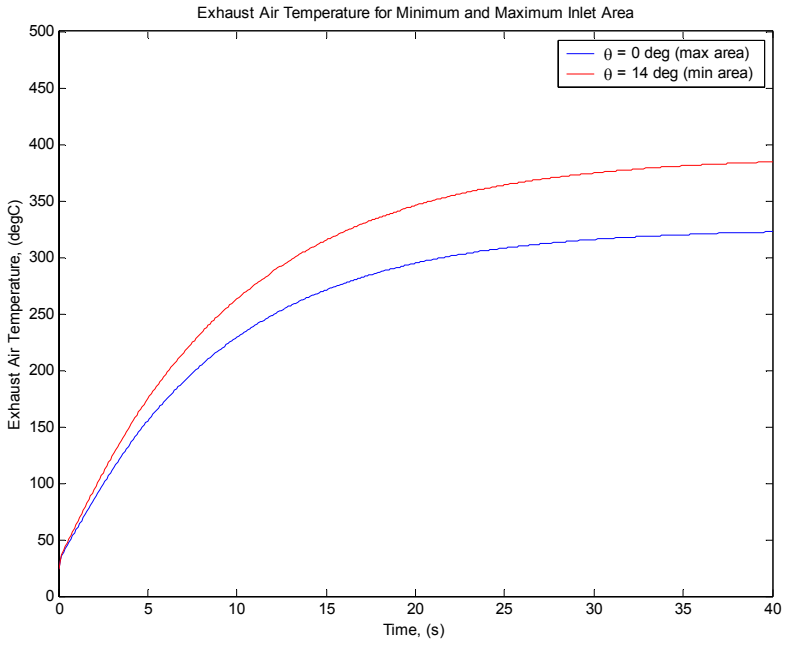

Figure 14: Exhaust Air Temperature for Minimum and Maximum Inlet Area

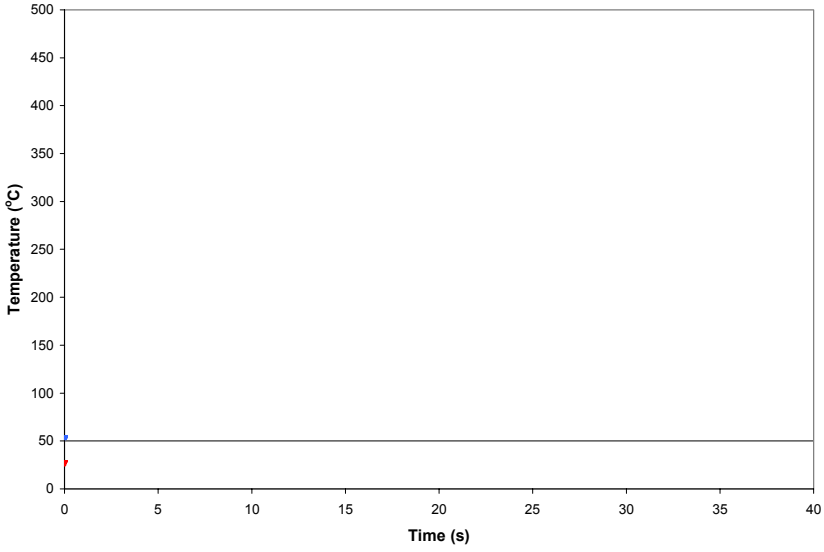

Figure 15: Experimental Thermal Data for Minimum and Maximum Inlet Area

It is apparent from Figure 14 that the magnitude of the simulated temperature was only about 25-30°C less than the recorded temperature—an error of 5-7%. The simulation demonstrates a remarkable correlation with the data. There are several possible sources for the error in the simulation with the most likely source being temperature rise in the fluid due to flow friction. This explanation seems very feasible especially when examining the thermocouple data. In the data presented in Figure 7, which provided the thermal data for the fully opened configuration, it was seen that the initial temperature of the air was about 50°C. Each of these tests was run with the motor already at steady state, which suggests that the temperature rise of the fluid as it flowed through the heat gun was about 25°C before it reached the heating element. This would provide the 25°C bias that is seen in the simulation versus the actual data. This hypothesis is also supported by the use of dissipative elements in the model of the fluid circuit without also including their entropy contribution to the system. With a 5-7% effect on the result of the simulation, it appears that these losses are important to the thermal dynamics of the system.

The final variable considered in order to validate the model was the temperature of the coil. Although no data was taken for the coil temperature, the color of the wire can be used to qualitatively approximate the steady-state coil temperature. It was observed during thermal testing that the coil glowed in the medium to light orange color range. The following table provided by Process Associates of America indicates the possible range of temperatures corresponding to this color range [8].

Table 1: Metal Color versus Temperature

Table removed due to copyright considerations.
See reference [8].

From this table it is evident that the temperature of the coil was probably in the range of 890-940°C.

The temperature of the coil as predicted by the mathematical model is shown in Figure 16. With a bulk heat transfer coefficient of 4.5 W/K the simulation predicts coil temperatures of 850 and 910°C for the fully opened and fully restricted flows respectively. According to Table 1, these temperatures would result in a coil color in the range of salmon to medium orange, which is indeed the case.

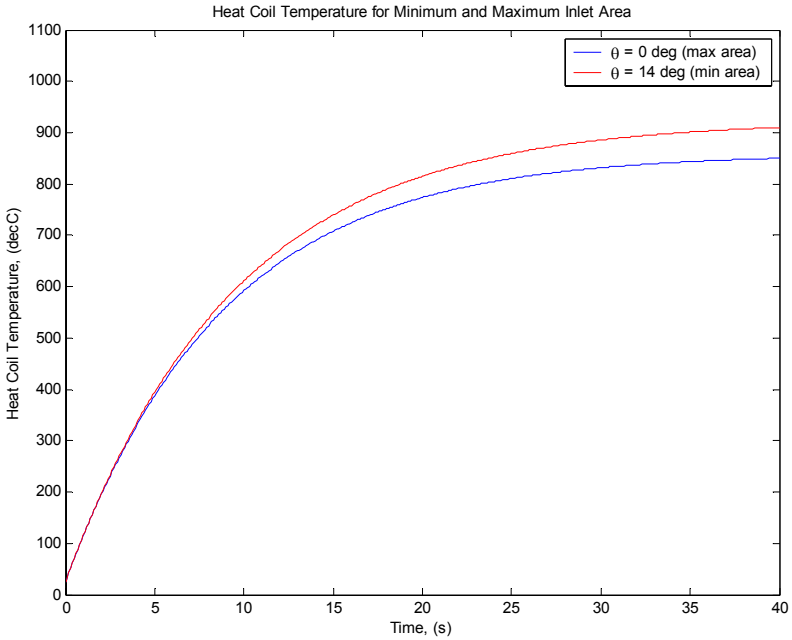

Figure 16: Temperature of Heating Coil for Minimum and Maximum Inlet Area

5 Conclusion

Although the heat gun initially seemed very complicated due to the coupling between multiple domains, it was found that the lack of energy storage elements in the system resulted in a deficiency of system dynamics. From the constitutive equations for the heat gun it is apparent that the fluid flow exhibits first order behavior and that the thermal behavior depends on both the time constant of the flow rate and on the thermal time constant of the heat coil. However, the time constant of the flow rate is so small compared to the thermal time constant that its contribution is not even apparent in the thermal results of the system model. Because of this, the mechanical, electrical, and fluid flow elements of the system can essentially be treated as a zero order system with complicated static coupling between domains.

While the dynamics of the system were relatively uninteresting, the coupling between domains led to a rigorous analysis of domain interactions and provided tremendous insight into non-conservative couplers. In addition, the inability of the model to fully predict the exhaust gas temperatures led to further insight about system dynamics that were not included in the model. A more complete model would attempt to alleviate this problem by including the entropy generated by flow restrictions in the overall temperature increase in the system.

Overall, the dynamic model was very successful at demonstrating the behavior of this device in all four domains. Unfortunately, the system could not be characterized entirely through measurement and analysis and some values, such as the effective length of the

flow restriction and the convection coefficient, were determined simply through trial and error. However, experimental results agreed completely with the final simulated results, with the only major discrepancy being the exhaust air temperature as discussed previously. With this major discrepancy between the results accounted for, the model appears to provide a complete picture of the system.

References

[1] "Universal Motors". University of Michigan, Mechanical Engineering, ME 350 Webpage. Accessed 12/04/2002. http://www.engin.umich.edu/labs/csdl/ME350/motors/ac/universal/index.html.

[2] Brown, Forbes T. *Engineering System Dynamics: A Unified Graph-Centered Approach*. New York: Marcel Dekker Inc. 2001.

[3] Wright, Terry. *Fluid Machinery: Performance, Analysis, and Design*. New York: CRC Press. 1999.

[4] "Centrifugal Wheel Designs". Lau Industries Inc., Barry Blower Central Webpage. Accessed 12/08/2002. http://www.barryblower.com/centrifugal.htm.

[5] Fox, R.W. and A.T. McDonald. *Introduction to Fluid Mechanics: Fifth Edition*. New York: John Wiley and Sons, Inc. 1997.

[6] Logan, Earl Jr. *Turbomachinery: Basic Theory and Applications*, *Second Edition*. New York: Marcel Dekker, Inc. 1993.

[7] Incropera, F.P and D.P. DeWitt. *Fundamentals of Heat and Mass Transfer: Fourth Edition*. New York: John Wiley & Sons. 1996.

[8] "Metal Temperature by Color," Process Associates of America. 1995-2002. Website accessed 12/09/02. http://www.processassociates.com/process/heat/metcolor.htm